Korean J. Chem. Eng., 33(9), 2659-2667 (2016)
DOI: 10.1007/s11814-016-0119-1

pISSN: 0256-1115
eISSN: 1975-7220

Synthesis of acrylic-lignosulfonate resin for crystal violet removal from aqueous solution

Wenjing Xu†, Wensheng Zhang, Yan Li, and Wei Li

School of Science, Jiaozuo Teachers' College, Jiaozuo Engineering Technology Research Center of Separation and Adsorption Materials, Jiaozuo, Henan 454000, China
(*Received 20 October 2015 • accepted 30 April 2016*)

Abstract−A new acrylic-lignosulfonate resin (ALR) was obtained by radical polymerization using calcium lignosulfonate (LS-Ca) and acrylic acid (AA) as raw materials. ALR was characterized using FT-IR, SEM, TG-DSC and N_2 adsorption–desorption surface area and pore size analyzer. Batch adsorption, including initial concentration, time, pH, dosage and temperature on the adsorption of crystal violet (CV) by ALR, was systematically studied. The ALR contained porous structure and the specific surface area of ALR was 190.55 m^2/g with average pore diameter 11.34 nm. The kinetic and equilibrium data fitted into the pseudo-second-order model and Freundlich isotherm model, respectively. The adsorption process was slightly influenced in the range of pH=3-12. The maximum adsorption capacity of CV was found to be as high as 150.40±4.80 mg/g for 24 h at 25 °C. Thermodynamic parameters were evaluated, and their values indicated that adsorption of CV on ALR was an exothermic process and spontaneous.

Keywords: Adsorption, Calcium Lignosulfonate, Crystal Violet, Modification, Wastewater

INTRODUCTION

Many industries (textile, leather, paper, printing, food, paint, etc.) have to use dyes or pigments to color their products. The release of dyes from these industries, resulting in generation of colored wastewater, is a major environmental problem [1-3]. The colored wastewater would compromise aquatic life because the photosynthetic rate of aquatic flora is impeded by preventing light penetration [4,5]. Dye residues or their metabolites could have toxic, carcinogenic, and mutagenic effects on flora, fauna, and human beings [6]. This dictates that the treatment of dye-contaminated effluents is necessary before being released into the environment or water bodies.

Various processes of dyes removal are used, such as membrane separation, flocculation-coagulation, chemical oxidation and photocatalytic processes, electrochemical techniques, and so on [7-9]. Of special interest, adsorption is one of the most effective and attractive methods for the treatment of dye-containing wastewater [10,11].

Adsorbents of various types have been employed to remove dyes from aqueous solutions [12-16]. Various types of activated carbon and modified cellulose have been used to remove a wide range of dyes from water. However, the practical application of these adsorbents is restricted due to the regeneration difficulty and high operation cost [14,17,18]. Polymeric resin has been widely used in wastewater treatment owing to its high adsorption efficiency, easy desorption and operation, long service life, etc. [19,20]. In particular, the polymeric resin modified by functional group could improve the adsorption properties of the resin [21,22].

Lignin, which generally exists in the cell walls of terrestrial plants, is the second most abundant natural polymer throughout the world after cellulose [23]. Lignin is well known as a waste by-product from pulp and paper industries. About 90-95% of industrial lignin is discharged directly into water resources, with rest predominantly burnt off as fuel, leading to a waste of natural resource and pollution of the environment [24].

The composition and structural units of lignin differ depending on the source of biomass from which lignin is extracted. In the paper industry, different types of lignin are obtained as waste by-products depending upon the pulping process. Calcium lignosulfonate (LS-Ca) is usually derived from the pulping of the acid process. Structurally, LS-Ca is an aromatic three-dimensional polymer containing a number of functional groups such as phenolic hydroxyl, alcoholic hydroxyl, carbonyl, methoxyl, sulfonic acid group and conjugated double bonds [25], which endows it and its derivates with the ability to adsorb many kinds of dyes. There are a number of reports on the treatment of wastewater using LS-Ca, lignin or modified lignin [26-30]; however, the report of synthetic polymeric resin modified by LS-Ca is still rare.

In this paper, acrylic resin was modified by radical polymerization with LS-Ca. The introduction of phenolic hydroxyl and sulfonic acid groups into the resin backbone enhanced the interaction and adsorption capacity between the acrylic resin adsorbent and dyes. The resulting adsorbent, referred to acrylic-lignosulfonate resin (ALR), was used to remove crystal violet (CV) from aqueous solution. Fundamental adsorption properties, including the adsorbent dosage, the initial pH value, the contact time, temperature and the initial concentration of CV in aqueous solution were all investi-

†To whom correspondence should be addressed.
E-mail: xwj900128@126.com

gated and the adsorption mechanism was also proposed.

MATERIALS AND METHODS

1. Chemicals and Instrumentation

The chemicals including acrylic acid, crystal violet, acetone, methanol and 1,4-dioxane were purchased from Chemical Reagent (Shanghai, China) as analytical reagent grade. Calcium lignosulfonate (96%) was purchased from Shanghai Jingcun Biochemical Technologies Co. and was used without any further purification. Ethylene glycol dimethacrylate (EGDMA, cross linker) and Potassium peroxydisulfate (KPS) were purchased from Aladdin Chemicals (Shanghai, China). KPS was recrystallized before use. All solutions were prepared using distilled water.

Fourier transform infrared (FT-IR) spectroscopy of the samples was recorded on a spectrum 100 FT-IR spectrophotometer (Perkin-Elmer, USA) using a KBr disk method and scanned in the range of 4,000-400 cm^{-1}. The SEM images were examined with JSM-6700F scanning electron microscopy (JEOL Ltd., Japan). TG-DSC was performed for powder samples using an STA 449F3 Jupiter Instrument (Netzsch Ltd., Germany). The specific surface area and pore size of the adsorbents were carried out at 77 K (boiling point of nitrogen) with the aid of volumetric adsorption analyzer (ASAP 2420, Micromeritics, USA). Established BET and BJH techniques were employed for area determination and pore calculation. CV concentration of the test samples was analyzed using a UV-vis spectrophotometer (Lambda 35, Perkin-Elmer, USA).

2. Preparation of ALR

The ALR were prepared by radical polymerization method (as shown in Fig. 1). LS-Ca powder was separately dissolved in 10 ml of distilled water to get a LS-Ca solution (3.0% w/v), AA (0.70 g) and EGDMA (3.64 g) were dissolved in 10 ml of 1,4-dioxane to get another mixture solution. Then, the above two solutions were mixed and the pH was adjusted to 4.0 using 0.1 mol/L HCl. After KPS (0.064 g) was added as an initiator, the glass tube was sealed and stirred in a water bath maintained at 60 °C for 24 h. After the reaction was completed, the mixture was cooled to room temperature and dried in a vacuum drying oven at 50 °C. The polymer obtained was crushed to a particle size of 100-200 mesh and the sieved particles were washed with methanol repeatedly till neutral. Finally, the obtained polymer (ALR) particles were dried under vacuum at 50 °C for 24 h for further use. The polymer unmodified with calcium lignosulfonate (AcR) was also prepared using an identical procedure without the addition of LS-Ca.

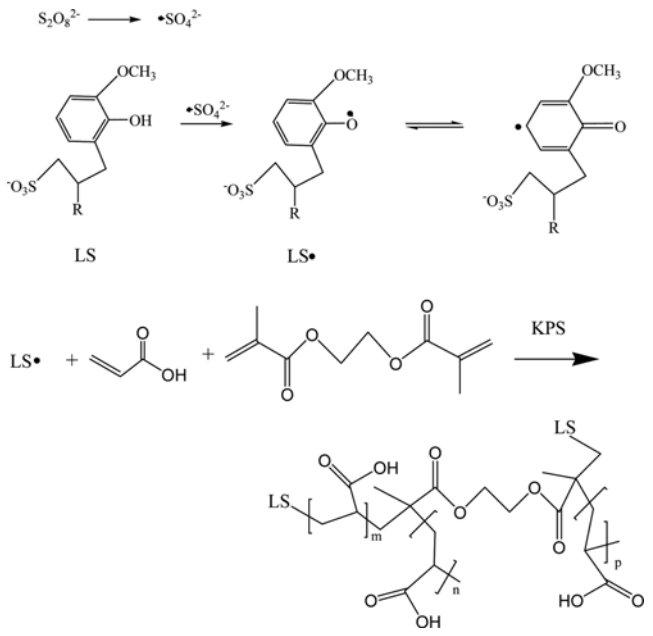

Fig. 1. The synthetic diagram of ALR.

3. Swelling Ratio of ALR

Swelling ratio of ALR was measured in aqueous solution. The ALR adsorbents were weighed (W_0) and immersed in 200 mL of aqueous solution at 25 °C. after 24 h, the swollen adsorbents were taken out and weighed (W_t) after excess water was removed with a filter paper. Swelling ratio (the water adsorption capacity) S_w (g/g) was calculated by the following formula:

$$S_w(g/g) = \frac{W_t - W_0}{W_0} \quad (1)$$

4. Batch Adsorption

The batch adsorption involved mixing adsorbent with CV aqueous solution. The mixture was agitated at 150 rpm in a SHA-B water bath constant temperature shaker to reach the equilibrium. The effect of pH on the adsorption was studied in the range of 3.0-12.0 that was adjusted with 0.10 mol/L HCl or NaOH solution at 25 °C. The effect of dosage on the adsorption was determined with different adsorbent dosage of 50-250 mg with 50 mL CV solution at 200 mg/L. Adsorption isotherms were studied at different initial CV concentration (30-250 mg/L) 50 mL with an ALR dosage of 50 mg under temperature of 25 and 30 °C, respectively. Adsorption kinetics were carried out at 25 °C with 100 mg adsorbent and 100 mL of CV concentration (200 mg/L). The samples were collected at predetermined time intervals immediately. The concentration of CV was measured by UV-vis spectrophotometer at a wavelength of 580 nm. The adsorption amount (Q, mg/g) was calculated by the following formula:

$$Q = \frac{(C_0 - C) \times V}{m} \quad (2)$$

where C_0 (mg/L) and C (mg/L) are the initial and final concentrations of CV, respectively, V (L) is the volume of the solution, and m (g) is the mass of adsorbent, respectively. The CV removal percentage was calculated by the following formula:

$$\%\text{Re moval} = \frac{C_0 - C}{C_0} \times 100 \quad (3)$$

5. Desorption

The desorption and recyclability of the ALR was measured at 25 °C. 0.150 g of ALR was added into 50 mL of 200 mg/L CV solutions for 24 h, then taken out from the solutions. The desorption and regeneration of ALR loaded by dyes were performed by placing these ALR into 50 mL of several different solvents (the mixture of ethanol and water solutions) under agitating at 25 °C for 2 h. The regenerated adsorbents were used for another adsorption

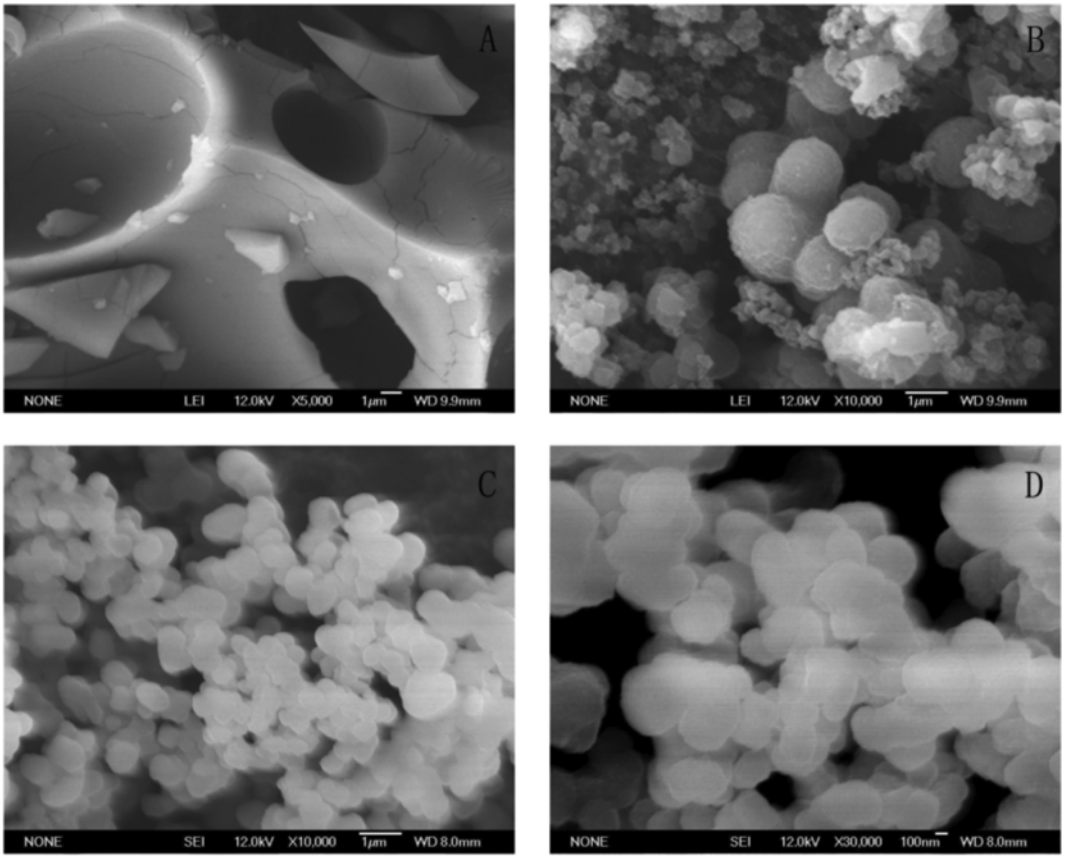

Fig. 2. SEM images of (A) LC-Ca, (B) AcR, (C) ALR, and (D) ALR (magnification: ×30,000).

in the subsequent cycles.

RESULTS AND DISCUSSION

1. Surface Morphology and Specific Surface Area Analysis

The SEM images (Fig. 2) were used to study the surface morphology of LS-Ca, AcR and ALR before and after the modification. It is observed that the surface of LS-Ca is smooth, while the surface of AcR and ALR are porous and rough. As can be seen, the AcR (Fig. 2(b)) exhibits as non-uniform and amorphous plates/particles with some agglomeration. Inspiring, the ALR (Fig. 2(c)) exhibits a porous structure with relatively uniform ball-like particles that might be due to the function of surface active agent (LS-Ca), and the ALR (Fig. 2(d)) exhibits rough surface on the ball-like particles, which will increase its surface area and will be beneficial for the adsorption of CV from aqueous solution.

The textural characteristics of ALR and AcR are shown in Table 1. It can be observed that the specific surface area is 190.55 m^2/g for ALR, which is significantly higher than that of AcR (142.59 m^2/g), and the total pore volume of ALR (0.4831 cm^3/g) is significantly higher than that of AcR (0.3753 cm^3/g), while the average pore diameter of ALR (11.34 nm) is slightly lesser than that of AcR (12.00 nm). The increase in surface area and total pore volume of ALR was primarily due to the presence of LS-Ca, which made the pore become smaller and more during the preparation of the ALR. It is ascertained that the surface area and total pore volume are important textural parameters to evaluate the sorption capacity of an adsorbent [3,31], and it is expected that excellent textural properties of

Table 1. Textural properties of AcR and ALR

Adsorbent	Specific surface area (m^2/g)	Total pore volume (cm^3/g)	Average pore diameter (nm)
AcR	142.59	0.3752	12.00
ALR	190.55	0.4831	11.34

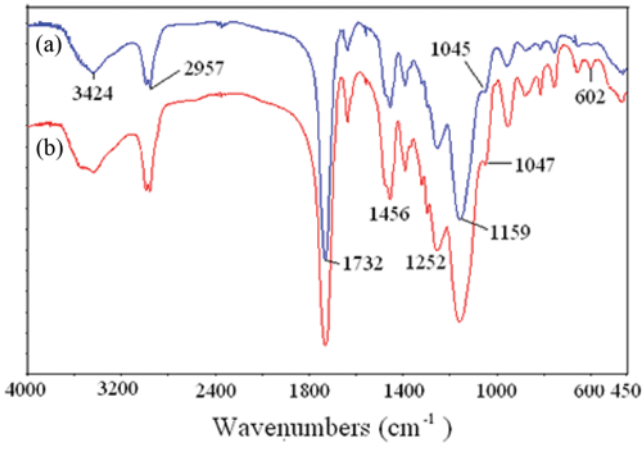

Fig. 3. FT-IR spectra of (a) AcR, (b) ALR.

ALR would improve its adsorbing capacities for CV dye from aqueous solutions compared to unmodified AcR.

2. FT-IR Analysis

The FT-IR spectra of samples are shown in Fig. 3. The peaks at 2,957, 1,732, 1,456 cm^{-1} correspond to C-H symmetric and asymmetric stretching vibration, C=O stretching vibration, C-H in-plane bending vibration, respectively. The peaks at 1,252 and 1,159 cm^{-1} are assigned to C-O stretching vibration. The appearance of new bands of ALR at 602 cm^{-1} should be attributed to C-S bending vibration [32]. The peaks at 3,424 cm^{-1} can be assigned to hydroxyl group stretching which changed broad at ALR compared to AcR, as should be attributed to phenolic hydroxyl group from LS-Ca. The peak at 1,045 cm^{-1} can be assigned to alkyl ether bond vibration for AcR which appears at 1,047 cm^{-1} for ALR, as should be attributed to sulfonate group from LS-Ca. All the results confirmed that EGDMA, AA and LS-Ca had participated in polymerization reaction in the presence of initiators KPS and the adsorbent ALR was successfully synthesized, which will increase the number of active sites in the surface of ALR and will be benefit for the adsorption of CV from aqueous solution compared to AcR.

3. Thermal Analysis and Swelling Ratio of ALR

The thermogravimetric curves of LS-Ca, AcR and ALR are depicted in Fig. 4(a). Compared with LS-Ca, the ALR and AcR exhibited higher thermal stability. Furthermore, LS-Ca (<181.1 °C), ALR (<305.2 °C) and AcR (<290.3 °C) could not be easily decomposed within its initial temperature range, and only 7.66% (LS-Ca) weight loss around 100 °C resulted from the few free water of samples. The LS-Ca sample was pyrolyzed over a broad temperature range from 181.1 to 400 °C, as observed in the weight loss. With the temperature increased to 400 °C, significant weight losses of ALR (81.09%) and AcR (83.42%) could be seen, respectively. At 400 °C, the remaining mass for ALR and AcR might be attributed to the thermal resistance of residual carbon by calcining polymers [33]. It is clear that the chemically modified samples (ALR) by LS-Ca are more thermally stable compared to the unmodified samples (AcR).

The DSC, TG and DTG curves of ALR are depicted in Fig. 4(b). It is observed that exothermal ehavior of ALR was divided into two-stages: the exothermic process under 305.2 °C was not associated with weight loss, indicating that the pre-change process of ALR was a physical process, while the exothermic process above 305.2 °C was accompanied by weight loss indicating that was a chemical decomposition process. Fig. 4(b) shows that the weight loss of ALR completed by only one step, indicating that the ALR was pure substance after chemically modified by LS-Ca, and not a physical mixture. Swelling ratio of ALR was 1.262 g/g at 25 °C for 24 h.

4. Effect of Initial Solution pH and Adsorbent Dosage

The pH of solution is an important parameter in the adsorption process as it may affect the level of electrostatic or molecular interaction between the adsorbent surface and the adsorbate owing to charge distribution on the material. To optimize the pH for maximum removal efficiency, adsorption experiment was conducted in the initial pH range from 3 to 12 at an initial CV concentration of 200 mg/L with a ALR dosage of 100 mg/100 mL. The results are shown in Fig. 5. It is clear that the adsorption capacity of CV in the range of pH studied presented a slight increase with increasing the pH, but no significant differences were observed. A similar behavior has been reported by other CV adsorptions studies [34,35]. The adsorption capacity and the percentage removal of CV by ALR arrived around 170 mg/g and 85% for 48 h and 150.40 mg/g and 75.2% for 24 h at 25 °C, respectively, which is higher compared to the reports for other types of adsorbents [34,35].

To investigate the effect of adsorbent amount, the adsorption of CV was conducted at five different adsorbent dosages at an initial

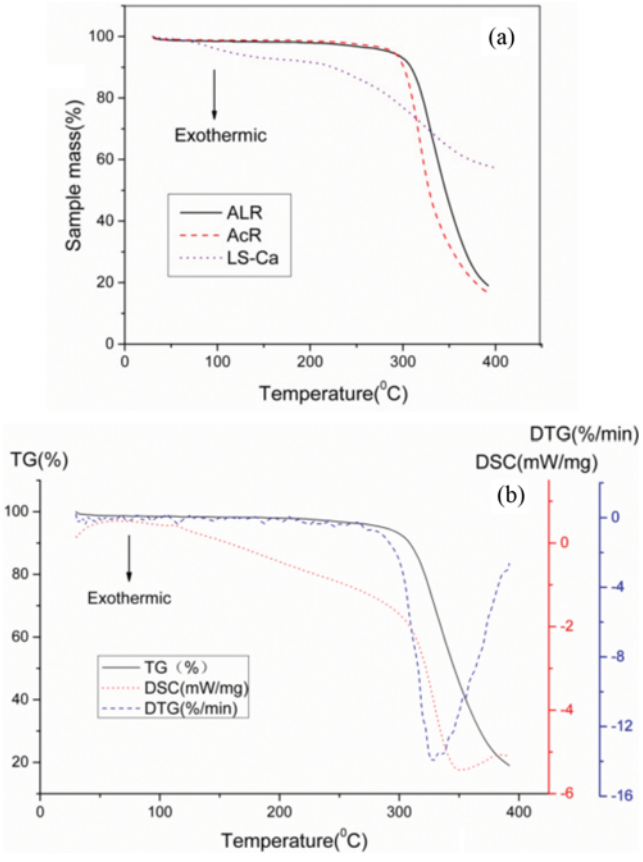

Fig. 4. (a) TG of ALR, AcR and LS-Ca, (b) DSC, TG and DTG of ALR.

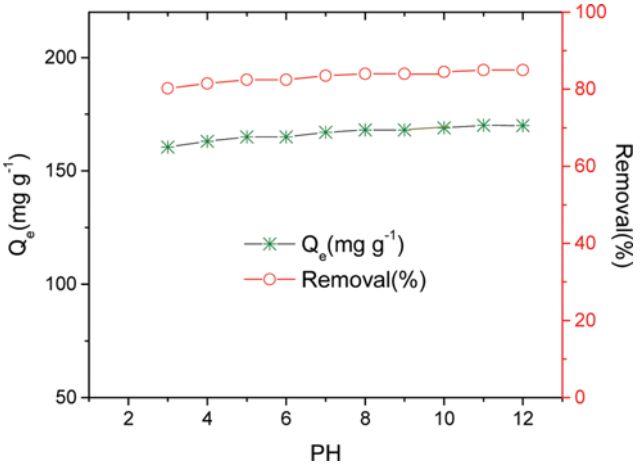

Fig. 5. Effect of pH on the adsorption capacity of CV by ALR at 298 K for 48 h.

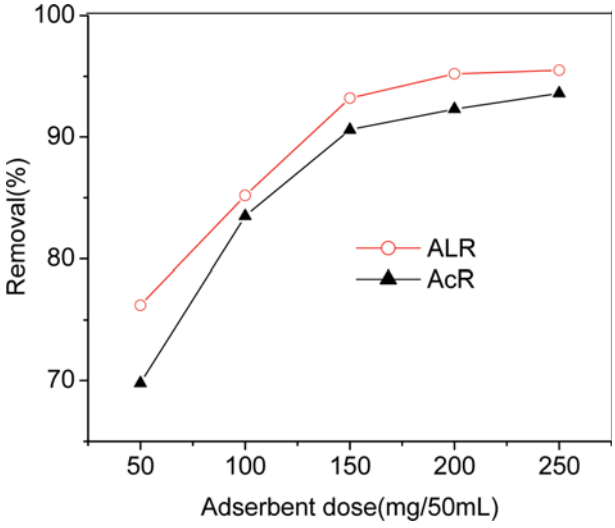

Fig. 6. Effect of ALR and AcR dosage on the adsorption percentage of CV at 298 K for 24 h.

CV concentration of 200 mg/L and 25 °C for 24 h. Fig. 6 shows that the adsorption percentage of CV increased from 75.2±2.4% to 95.5±2.1% as the ALR dosage increased from 50 to 250 mg/50 mL, which could be assigned to the increase of surface area and number of active sites with increasing of ALR dosage [32]. Similar behavior for the effect of adsorbent dosage on the adsorption percentage of CV was reported in the literature for other types of adsorbents [34,35]. When the ALR dosage increased from 150 to 200 mg/50 mL, the adsorption percentage only increased 2.0%. Therefore, the suitable ALR dosage for the removal of CV should be 150 mg/50 mL for 24 h. However, the adsorption percentage of CV increased from 69.8±2.4% to 93.6±2.1% as the AcR dosage from 50 to 250 mg/50 mL, lower than ALR.

5. Adsorption Kinetics

Adsorption kinetics provides valuable information about the mechanism of adsorption and characteristics of CV by ALR. Fig. 7 shows the kinetic curves for CV adsorption onto ALR at the initial concentration of 200 mg/L at 25 °C. The adsorption amount (Q_t) of CV increased rapidly with time within the first 100 min, and then the adsorption of CV on ALR was slow within 100-480 min. After that, there was a little adsorbed amount of CV as time went on. To further understand the adsorption kinetics, the pseudo-first-order model [36] and pseudo-second-order model [37] were both applied to fit the kinetic data.

$$\text{Pseudo-first-order model: } Q_t = Q_e(1-e^{-k_1 t}) \quad (4)$$

$$\text{Pseudo-second-order model: } Q_t = \frac{Q_e^2 k_2 t}{1+Q_e k_2 t} \quad (5)$$

And their linear equations:

$$\text{Pseudo-first-order model: } \lg(Q_e - Q_t) = \lg Q_e - \frac{k_1 t}{2.303} \quad (6)$$

$$\text{Pseudo-second-order model: } \frac{t}{Q_e} = \frac{1}{k_2 Q_e^2} + \frac{1}{Q_e} t \quad (7)$$

where Q_e and Q_t (mg/g) are the adsorbed amounts of CV at equilibrium and at contact time t (min), respectively; k_1 (min^{-1}) and k_2 (g mg^{-1} min^{-1}) are the rate constants. The kinetic parameters in the above linear models were determined by plotting $\log(Q_e - Q_t)$ versus t and t/Q_t versus t, respectively.

The fitting results of adsorption kinetics data by linear and nonlinear pseudo-first-order, and pseudo-second-order models are shown in Figs. 7, 8 and Table 2. In Table 2, the calculated correlation coefficient values (R^2) for pseudo-first-order (0.9852 and 0.9984 for linear fit and nonlinear fit, respectively) and pseudo-second-order (0.9981 and 0.9998 for linear fit and nonlinear fit, respectively) kinetics are found to be greater than 0.98, which shows the applicability of both these kinetic models. However, as seen in Table 2, the predicted adsorption capacities (Q_e=144.93 mg/g and 144.91 mg/g for linear fit and nonlinear fit, respectively) by pseudo-second-order were in accordance with the experimental value ($Q_{e,cal}$= 150.40±4.80 mg/g), but the predicted Q_e values (97.17 mg/g and 128.08 mg/g for linear fit and nonlinear fit, respectively) by pseudo-

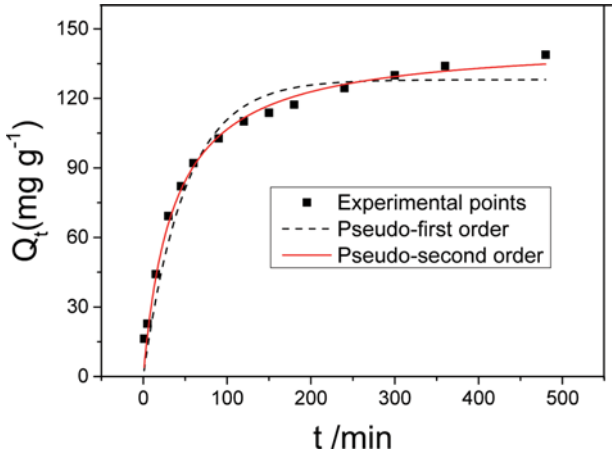

Fig. 7. Adsorption kinetics and the nonlinear fitting results by pseudo-first-order and pseudo-second-order models.

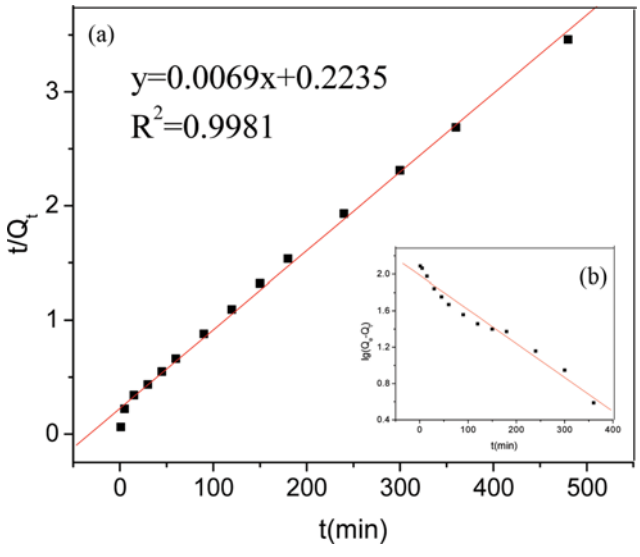

Fig. 8. Adsorption kinetics and the linear fitting results by pseudo-second-order (a) and pseudo-first-order (b) models.

Table 2. Kinetic parameters for the adsorption of CV by ALR

Models	Pseudo-first-order model			Pseudo-second-order model			$Q_{e,cal}$ (mg/g)
Parameters	R_1^2	Q_e (mg g^{-1})	K_1 (min^{-1})	R_2^2	Q_e (mg g^{-1})	K_2 (g mg^{-1} min^{-1})	
Nonlinear fit	0.9984	128.08	2.00×10^{-2}	0.9998	144.91	1.92×10^{-4}	150.40±4.80
Linear fit	0.9852	97.17	8.61×10^{-3}	0.9981	144.93	2.13×10^{-4}	

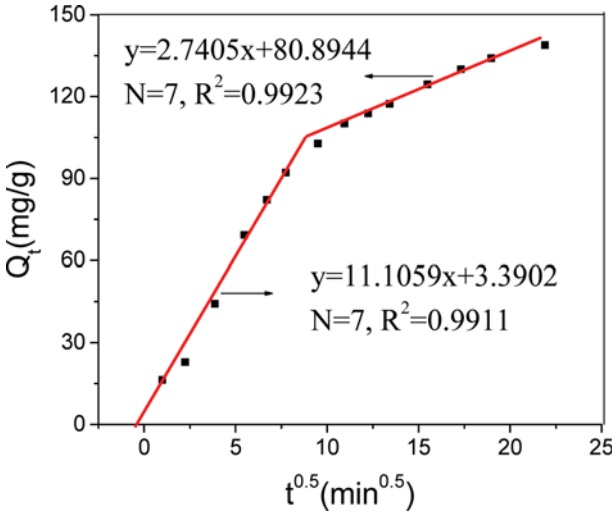

Fig. 9. Intraparticle diffusion model for the adsorption of CV on ALR.

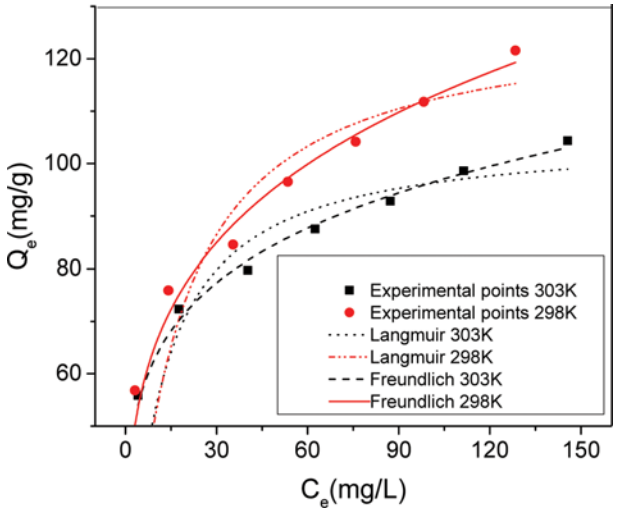

Fig. 10. Adsorption isotherms and the fitting results by Langmuir and Freundlich models.

first-order are not close to the experimental values. That indicates for the entire sorption period studied, the pseudo-second-order expression better predicts the sorption kinetics than the pseudo-first-order model, which means that the rate adsorbed CV on ALR is heavily dependent on the amount of CV on the ALR surface [38].

The kinetic experimental data were also applied to the intraparticle diffusion model, which is given in the following form [38].

$$Q_t = k_p t^{1/2} + C \quad (8)$$

where k_p (mg g^{-1} $h^{-0.5}$) is intraparticle diffusion rate constant, which can be obtained from the slope of Q_t vs $t^{1/2}$ and C (mg/g) is the intercept. If intraparticle diffusion is a rate-limiting step, Q_t vs $t^{1/2}$ should be linear and the plot should pass through the origin. Fig. 9 shows the plot of the amount of CV adsorbed (Q_t) versus the square root of time ($t^{1/2}$). The plot has two linear sections, indicating that the adsorption processes had more than one sorption rate [3,5,39]. Fig. 9 shows that the adsorption process of CV on ALR included two stages and each stage was ascribed to each linear portion of the plots. The initial linear portion, the faster stage, was attributed to the process in which dye molecules diffused to the surface of adsorbents [3,5,39]. The second part of the plots was assigned to intra-particle diffusion, a slower process [3,5,39]. The plot in this case is not linear over the whole time range and does not pass though the origin, indicating that intraparticle diffusion was applicable to this system to a certain extent but was not the only rate-controlling step in the adsorption [38].

6. Adsorption Isotherm

The adsorption isotherms of CV on ALR at two temperatures are displayed in Fig. 10. Obviously, the equilibrium adsorption amount (Q_e) increased significantly along with the increase of CV equilibrium concentration (C_e) in aqueous solution.

The isotherms in this study were analyzed by using the Freundlich and Langmuir isotherm equations. The Langmuir adsorption isotherm is based on a monolayer surface coverage of the adsorbate on the adsorbent that contains a finite number of adsorption sites of uniform adsorption energies, whereas the Freundlich isotherm assumes non-ideal sorption on heterogeneous surfaces and multiple adsorption layers. Langmuir and Freundlich isotherms are expressed by the following equations [38]:

$$\text{Langmuir: } Q_e = \frac{Q_m b C_e}{1 + b C_e} \quad (9)$$

$$\text{Freundlich: } Q_e = K_F C_e^{1/n} \quad (10)$$

where Q_e (mg/g) is the amount of CV adsorbed on the adsorbent, C_e (mg/L) is the equilibrium CV concentration, Q_m represents a saturated adsorption capacity, b (L/mg) is the Langmuir adsorption constant, K_F (L/g) is the Freundlich constant indicating the adsorption capacity, n is the heterogeneity factor representing the adsorption intensity.

The fitting results of adsorption equilibrium data by Langmuir and Freundlich models are shown in Fig. 10 and Table 3. A nonlinear method characterized with successive interactions calculated by the orthogonal distance regression method was used to fit the equilibrium data. Similarly, interactions were evaluated with the aid of the Simplex method, based on the nonlinear fitting facilities of the Microcal Origin 9.1 software. A reduced chi-sqr (X^2) and a correlation coefficient (R^2) were used to evaluate the models used

Table 3. Fitting results of adsorption isotherms by Langmuir and Freundlich models

T (K)	Langmuir				Freundlich			
	X^2	R_L^2	Q_m (mg g^{-1})	b (L mg^{-1})	X^2	R_F^2	n	K_F (mg g^{-1})
298	37.81	0.9884	128.27	0.06899	6.24	0.9981	4.286	38.43
303	24.17	0.9921	105.52	0.1033	2.07	0.9993	5.504	41.68

in this study. X^2 is a measure of the difference between the theoretical amount of dye adsorbed by an adsorbent and the actual adsorption amount of dye measured experimentally.

As can be seen, the calculated correlation coefficient values (R^2) for Langmuir (0.9884 and 0.9921 at 298 K and 303 K, respectively) and Freundlich (0.9981 and 0.9993 at 298 K and 303 K, respectively) model are found to be greater than 0.98, which shows the applicability of both these isotherm models. However, the reduced chi-sqr (X^2) values for Freundlich model (6.24 and 2.07 at 298 K and 303 K, respectively) is obvious lower than Langmuir model (37.81 and 24.17 at 298 K and 303 K, respectively). The Freundlich model gave the lower X^2 values, indicating that the experimental adsorption capacity was closer to the theoretical adsorption capacity of the isotherm model and the adsorption of CV by ALR could be described better by Freundlich adsorption model at 298 K and 303 K, meanwhile the value of n>1 illustrated that the adsorption was favorable with strong adsorption intensity [38]. As to Langmuir model, the high X^2 values and low saturated adsorption capacities (Q_m=128.27 mg/g and 105.52 mg/g at 298 K and 303 K, respectively) compared with the experimental value (150.40±4.80 mg/g and 125.73±3.50 mg/g at 298 K and 303 K, respectively) indicated the adsorption did not follow well this model.

7. Thermodynamics Studies

Thermodynamic parameters of adsorption process, such as Gibbs free energy (ΔG^o), enthalpy change (ΔH^o) and entropy change (ΔS^o), were evaluated using the following equation [27,35].

$$\Delta G^o = -RT\ln K \quad (11)$$

$$\ln K = -\frac{\Delta H^o}{RT} + \frac{\Delta S^o}{R} \quad (12)$$

where R represents the universal gas constant (8.314 J K^{-1} mol^{-1}); T represents the absolute temperature (Kelvin); K represents the distribution coefficient equals to Q_e/C_e.

The effect of temperature on the adsorption of CV onto ALR is given from the plots and curves of the distribution coefficient values K versus T in Fig. 11. It can be found that K decreased with increasing temperature. According to Eq. (12), the parameters of ΔH^o and ΔS^o can be calculated from the slope and the intercept of the plot of lnK versus 1/T, respectively. The calculated values of thermodynamic parameters are presented in Table 4.

As can be seen, the R^2 values of the plots are closer to unity, which indicates that the calculated enthalpy and entropy values for ALR are reliable. The type of interaction between adsorbent and adsorbate can be classified by the magnitude of enthalpy change to a certain extent. Physical adsorption (e.g., hydrogen bonding) is generally <35 kJ/mol [27,40]. For adsorption of CV onto ALR, the magnitude of enthalpy change conformed to that of physical adsorption [27,40]. The enthalpy changes (ΔH^o) have negatives values, showing that the adsorption processes of CV onto ALR were exothermic. In addition, adsorption of CV onto ALR was spontaneous and favorable process at all the experimental temperatures as a result of negative values of ΔG^o. The negative values of ΔS^o signified a decrease in the randomness at the solid-liquid interface.

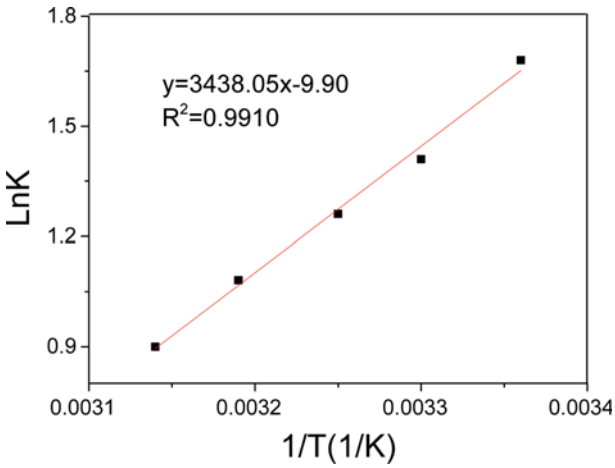

Fig. 11. Plot of lnK against 1/T for the adsorption of CV on ALR.

8. Desorption Studies

Desorption experiments were performed to determine the reusability of ALR for CV dye adsorption. The eluents tested for possible regeneration of dye-laden ALR adsorbents were 95% ethanol (20-100%)+water (20-80%), (Table 5). From Table 5, the mixture of 95% ethanol 80%+water 20% (v/v) and pH=1 exhibited the best desorption ability, desorbed 98.7% CV dye from ALR. This is termed the first cycle of adsorption/desorption. After three adsorption/desorption cycles, the recyclable adsorption behavior of ALR to CV was similar and the adsorption capacities of ALR decreased slightly; the dye removal of ALR to CV after one and three cycles was 93.2% and 84.6%.

Table 4. Thermodynamic parameters for the adsorption of CV on ALR

ΔH^o (kJ mol^{-1})	ΔS^o (J mol^{-1} K^{-1})	ΔG^o (kJ mol^{-1})				
		298 K	303 K	308 K	313 K	318 K
−28.58	−82.31	−4.16	−3.55	−3.23	−2.81	−2.38

Table 5. Desorption of dye-loaded ALR

Composition of eluent	Recovery (%)
95%ethanol	73.0
95%ethanol 80%+water 20%	73.6
95%ethanol 60%+water 40%	61.7
95%ethanol 40%+water 60%	35.9
95%ethanol 20%+water 80%	16.3
95%ethanol 20%+water 80%, pH=1	45.4
95%ethanol 80%+water 20%, pH=1	98.7

CONCLUSION

Acrylic resin modified by LS-Ca (ALR) was prepared successfully by radical copolymerization. The ALR contained porous structure with average pore diameter 11.34 nm. Used as a new adsorbent for the removal of CV from aqueous solution, it has great adsorption capacity for the adsorption of CV dye. The adsorption process was slightly influenced by the pH, and in the range of pH=3-12, the adsorption capacity of CV on ALR was found stronger in the solution. The adsorption capacity of CV by ALR arrived at 150.40± 4.80 mg/g for 24 h at 25 °C. The adsorption kinetics was found to follow pseudo-first-order model and the equilibrium data follows Freundlich isotherm model. The negative sign of ΔG^o confirmed the spontaneous nature of the adsorption process. The lower value of enthalpy (ΔH^o) indicated that hydrogen bonding interactions played an important role in adsorption process, and the negative sign of ΔH^o indicated that the adsorption process was exothermic. All these indicated that ALR is a promising sorbent of CV in water and the low cost, easy preparation and its efficient removal of CV from wastewater make ALR potent for the treatment of wastewater.

ACKNOWLEDGEMENTS

This work was supported by Foundation of Henan Scientific and Technological Committee (No. 162300410270), Science and Technology Research Key Program of Henan Educational Committee (No. 14B150056) and Foundation of Jiaozuo Scientific and Technological Bureau (No. 2014400038).

REFERENCES

1. S. Chowdhury, R. Mishra, P. Saha and P. Kushwaha, *Desalination*, **265**, 159 (2011).
2. S. Chakraborty, S. Chowdhury and P. D. Saha, *Clean Technol. Environ.*, **15**, 255 (2013).
3. M. A. Adebayo, L. D. T. Prola, E. C. Lima, M. J. Puchana-Rosero, R. Cataluna, C. Saucier, C. S. Umpierres, J. C. P. Vaghetti, L. G. Silva and R. Ruggiero, *J. Hazard. Mater.*, **268**, 43 (2014).
4. B. Royer, N. F. Cardoso, E. C. Lima, V. S. O. Ruiz, T. R. Macedo and C. Airoldi, *J. Colloid Interface Sci.*, **336**, 398 (2009).
5. N. F. Cardoso, E. C. Lima, I. S. Pinto, C. V. Amavisca, B. Royer, R. B. Pinto, W. S. Alencar and S. F. P. Pereira, *J. Environ. Manage.*, **92**, 1237 (2011).
6. P. Saha, S. Chowdhury, S. Gupta and I. Kumar, *Chem. Eng. J.*, **165**, 874 (2010).
7. X. Chen, L. Wan, Q. Wu, S. Zhi and Z. Xu, *J. Membr. Sci.*, **441**, 112 (2013).
8. A. Ahmad, S. H. Mohd-Setapar, C. S. Chuong, A. Khatoon, W. A. Wani, R. Kumar and M. Rafatullah, *Rsc. Adv.*, **5**(39), 30801 (2015).
9. M. Rafatullah, O. Sulaiman, R. Hashim and A. Ahmad, *J. Hazard. Mater.*, **177**, 70 (2010).
10. H. Gao, T. Kan, S. Zhao, Y. Qian, X. Cheng, W. Wu, X. Wang and L. Zheng, *J. Hazard. Mater.*, **261**, 83 (2013).
11. M. Vakili, M. Rafatullah, B. Salamatinia, A. Z. Abdullah, M. H. Ibrahim and K. B. Tan, *Carbohyd. Polym.*, **113**, 115 (2014).
12. N. F. Cardoso, E. C. Lima, B. Royer, M. V. Bach, G. L. Dotto, L. A. A. Pinto and T. Calvete, *J. Hazard. Mater.*, **241-242**, 146 (2012).
13. H. Gao, T. Kan, S. Zhao, Y. Qian, X. Cheng, W. Wu, X. Wang and L. Zheng, *J. Hazard. Mater.*, **261**, 83 (2013).
14. T. Ahmad, M. Danish, M. Rafatullah, A. Ghazali, O. Sulaiman and R. Hashim, *Environ. Sci. Pollut. Res. Int.*, **19**(5), 1464 (2012).
15. T. Ahmad, M. Rafatullah, A. Ghazali, O. Sulaiman and R. Hashim, *J. Environ. Sci. Heal. C*, **29**(3), 177 (2011).
16. L. W. Low, T. T. Teng, M. Rafatullah, N. Morad and B. Azahari, *Sep. Sci. Technol.*, **48**(11), 1688 (2013).
17. T. A. Khan, S. Dahiya and I. Ali, *Appl. Clay Sci.*, **69**, 58 (2012).
18. S. Irem, Q. M. Khan, E. Islam, A. J. Hashmat, M. A. Haq, M. Afzal and T. Mustafa, *Ecol. Eng.*, **58**, 399 (2013).
19. Q. X. Yao, J. J. Xie, N. Zeng, C. Ding and Y. Liu, *J. Funct. Mater.*, **45**, 129 (2014).
20. W. J. Xu, W. S. Zhang, W. Li, J. L. Yan, G. Y. Shen and J. Li, *J. Appl. Polym. Sci.*, **126**, 104 (2012).
21. W. J. Xu, W. S. Zhang and S. L. Zhang, *Petrochem. Technol.*, **43**, 698 (2014).
22. Y. F. Sun, Z. T. Liu, Z. H. Fei, Z. X. Li and R. Xing, *Acta Polym. Sin.*, **1**, 107 (2014).
23. X. Y. Guo, S. Z. Zhang and X. Q. Shan, *J. Hazard. Mater.*, **151**, 134 (2008).
24. M. B. Sciban, M. T. Klasnja and M. G. Antov, *Ecol. Eng.*, **37**, 2092 (2011).
25. X. J. He, J. J. Xie, Y. Wei, S. Li, K. Huang, X. Q. Han and H. Y. Zhang, *Sci. Silvae. Sin.*, **47**, 134 (2011).
26. L. G. Silva, R. Ruggiero, P. M. Gontijo, R. B. B. Pinto, E. C. Lima, T. H. M. Fernandes and T. Calvete, *Chem. Eng. J.*, **168**, 620 (2011).
27. Z. Li, Y. Kong and Y. Y. Ge, *Chem. Eng. J.*, **270**, 229 (2015).
28. R. Saad, Z. R. Hrapovic, B. Ahvazi, S. Thiboutot, G. Ampleman and J. Hawari, *J. Environ. Sci.*, **24**, 808 (2012).
29. M. B. Sciban, M. T. Klasnja and M. G. Antov, *Ecol. Eng.*, **37**, 2092 (2011).
30. Q. X. Yao, J. J. Xie, J. X. Liu, H. M. Kang and Y. Liu, *J. Polym. Res.*, **21**, 465 (2014).
31. V. Nair, A. Panigrahy and R. Vinu, *Chem. Eng. J.*, **254**, 491 (2014).
32. Y. Ge, D. Xiao, Z. Li and X. Cui, *J. Mater. Chem.*, **A2**, 2136 (2014).
33. J. M. Pan, B. Wang, J. D. Dai, X. H. Dai, H. Hang, H. X. Ou and Y. S. Yan, *J. Mater. Chem.*, **22**, 3360 (2012).
34. S. Jain and R. V. Jayaram, *Desalination*, **250**, 921 (2010).
35. R. Lafi, A. Fradj, A. Hafiane and B. H. Hameed, *Korean J. Chem. Eng.*, **31**, 2198 (2014).
36. Y. Zhan, X. Luo, S. Nie, Y. Huang, X. Tu and S. Luo, *Ind. Eng.*

Chem. Res., **50**, 6355 (2011).
37. B. H. Hameed, *Colloids Surf., A*, **307**, 45 (2007).
38. J. P. Zhang, X. Y. Lin, X. G. Luo, C. Zhang and H. Zhu. *Chem. Eng. J.*, **168**, 1055 (2011).
39. B. Royer, N. F. Cardoso, E. C. Lima, T. R. Macedo and C. Airoldi, *J. Hazard. Mater.*, **181**, 366 (2010).
40. C. L. Sun and C. S. Wang, *J. Mol. Struct.*, **956**, 38 (2010).